BIOCHEMISTRY
including biophysical chemistry & molecular biology

Article

pubs.acs.org/biochemistry

Biochemical and Structural Analysis of the Hyperpolarization-Activated K^+ Channel MVP

Amelia M. Randich, Luis G. Cuello,[†] Sherry S. Wanderling, and Eduardo Perozo*

Department of Biochemistry and Molecular Biology, The University of Chicago, Chicago, Illinois 60637, United States

ABSTRACT: In contrast to the majority of voltage-gated ion channels, hyperpolarization-activated channels remain closed at depolarizing potentials and are activated at hyperpolarizing potentials. The basis for this reverse polarity is thought to be a result of differences in the way the voltage-sensing domain (VSD) couples to the pore domain. In the absence of structural data, the molecular mechanism of this reverse polarity coupling remains poorly characterized. Here we report the characterization of the structure and local dynamics of the closed activation gate (lower S6 region) of MVP, a hyperpolarization-activated potassium channel from *Methanococcus jannaschii*, by electron paramagnetic resonance (EPR) spectroscopy. We show that a codon-optimized version of MVP has high expression levels in *Escherichia coli*, is purified as a stable tetramer, and exhibits expected voltage-dependent activity when reconstituted in liposomes. EPR analysis of the mid to lower S6 region revealed positions exhibiting strong spin−spin coupling, indicating that the activation gate of MVP is closed at 0 mV. A comparison of local environmental parameters along the activation gate for MVP and KcsA indicates that MVP adopts a different closed conformation. These structural details set the stage for future evaluations of reverse electromechanical coupling in MVP.

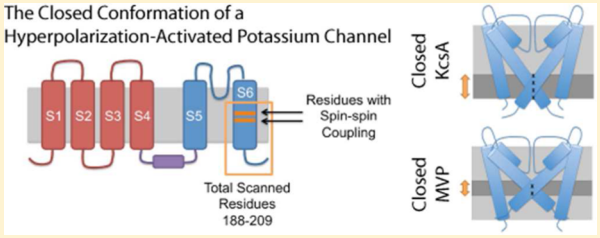

All cells depend upon ion channels to conduct ions across the cell membrane under specific conditions to shape their electrical behavior. Voltage-gated potassium (Kv) channels play crucial roles in physiological processes such as neuronal excitation and muscle contraction. Kv channels open in response to changes in the membrane potential by coupling four voltage-sensing domains (VSDs) to a central pore domain. In canonical, depolarization-activated Kv channels, the movement of the S4 helix of the VSD toward the extracellular side of the membrane during depolarization causes the pore domain to open and allows ion permeation.[1−3] Current structural and biochemical evidence from depolarization-activated channels supports the view that the S4−S5 linker couples the VSD and pore domains by acting as a rigid helical lever to hold the pore closed or open at hyperpolarizing potentials.[4,5] However, this mechanism fails to explain coupling in hyperpolarization-activated channels: despite conserving the molecular architecture of the Kv superfamily, they open when canonical family members are closed and close when canonical family members are open (Figure 1A,B). The mechanism of this inverse coupling has remained elusive in the absence of structural data. To open up new opportunities for structural and biophysical studies of this family, we have developed a biochemical preparation of an archaeal hyperpolarization-activated potassium channel from *Methanococcus jannaschii*, MVP.[6,7]

MVP poses an interesting case study for coupling between the VSD and the pore domain. MVP opens in response to hyperpolarization with half-maximal activation at −175 ± 33 mV and an apparent gating charge of 1.1 e[6] (Figure 1C). The VSD of MVP has the same orientation and senses changes in the polarity of the membrane potential in the same manner as canonical Kv channels, an important difference being that the MVP opens when the S4 helix moves downward (toward the intracellular side) and closes when the S4 helix moves upward (toward the extracellular side). The same observations have been made for the VSDs of the hyperpolarization-activated cyclic nucleotide-binding (HCN) channels and hyperpolarization-activated channels from plants,[6,8−10] suggesting that the key explanation for their reversed voltage sensitivity resides in an inverted coupling between the VSD and pore domains. Great strides toward understanding gating in HCNs have been made by expressing and characterizing HCN channels in oocytes or mammalian expression systems for electrophysiological studies. However, constraints on expression systems have limited structural studies to the isolatable and soluble cyclic nucleotide-binding domain (CNBD) located at the HCN C-terminus.[11]

Because of its relative structural simplicity and its prokaryotic origin, MVP exemplifies a minimalistic model for hyperpolarization-activated channels and is likely to be more amenable to spectroscopic and crystallographic studies than eukaryotic HCN channels. Like HCN channels, MVP is activated at hyperpolarizing voltages of less than −100 mV on a slower (0.2−2 s) time scale.[6,12] The moderate voltage dependence of MVP more closely resembles the equivalent of 4−6 e in HCNs than the 13 e for the highly voltage-dependent *Shaker* K^+ channel. There are a few critical differences between HCN channels and MVP. Unlike the HCN channels, MVP does not have a CNBD, and cyclic nucleotides do not modify its gating behavior or

Received: October 18, 2013
Revised: January 10, 2014
Published: February 3, 2014

 © 2014 American Chemical Society dx.doi.org/10.1021/bi4014243 | *Biochemistry* 2014, 53, 1627−1636

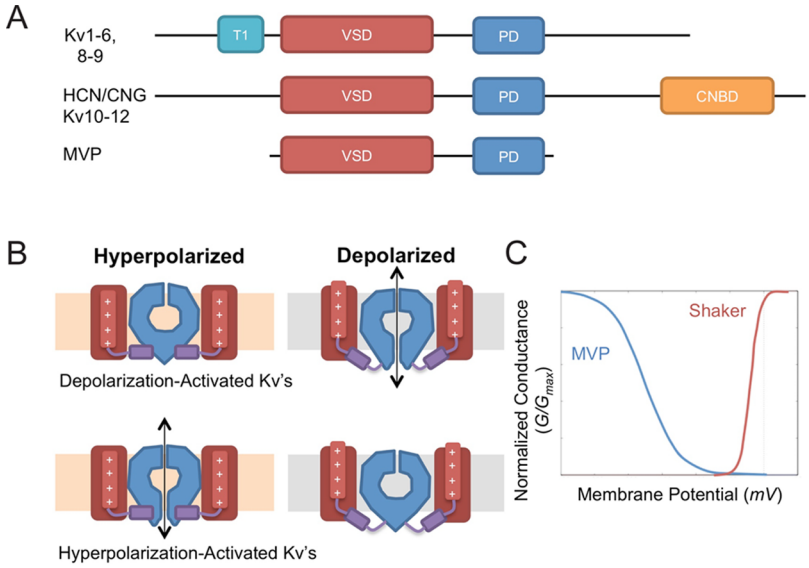

Figure 1. Canonical Kv and HCN channels share a common VSD and pore domain but are coupled inversely. (A) Schematic showing the shared domains of the voltage-gated ion channel family. (B) Hyperpolarization-activated channels exhibit inverse gating with respect to depolarization-activated channels: they are activated and open at hyperpolarizing potentials, when the conserved voltage sensor is in the down state. (C) GV curves displaying the voltage dependence of a hyperpolarization-activated channel (MVP) and a depolarization-activated channel (*Shaker*). The curves represent Boltzman fits to experimental data for MVP and *Shaker*.

conductance.[6] This is an important difference because both voltage and cyclic nucleotides activate HCNs[12] and the C-linker between the pore domain and the CNBD appears to make important functional contacts to the linker between the VSD and pore domain.[13,14] Moreover, MVP appears to exhibit a higher degree of sequence similarity to members of the Kv2 family, rather than the Kv10−12/HCN cluster. These observations suggest that MVP is a closer relative of the more thoroughly characterized Kv channels, such as *Shaker*, than the HCN channels and may serve as an important model system for improving our understanding of the mechanistic basis for electromechanical coupling between the VSD and pore domain.

In the interest of pursuing MVP as target for structural and biophysical studies, we have conducted an initial structural investigation of the activation gate in MVP using site-directed spin labeling and electron paramagnetic resonance (EPR) spectroscopy. A codon-optimized WT MVP construct is purified as a monodisperse peak via gel filtration chromatography and is stable in maltosides (DDM and DM) for weeks. Patch recordings of reconstituted MVP demonstrate kinetics and voltage dependence similar to those described in previous reports of exogenously expressed protein in yeast.[6] EPR measurements of the S6 helix demonstrate that reconstituted MVP is spectroscopically well behaved and that the pore domain is in the closed conformation at 0 mV, as expected for a hyperpolarization-activated channel. The availability of this stable, strongly expressing target will finally allow biochemical inroads into the molecular mechanism of inverse coupling and an understanding of electromechanical coupling in general.

EXPERIMENTAL PROCEDURES

Molecular Biology and Expression Test. The DNA encoding the codon-optimized synthetic gene sequence of MVP (MVP-s) was generously donated by S. Goldstein. In this synthetic construct, the native amino acid sequence is maintained while 62 of 209 archaeal codons are altered.[6] The gene was amplified by polymerase chain reaction (PCR) and cloned into pQE-32 (Qiagen), pQE-60, pGEX-6p-1 (GE Healthcare), pET15b (Novagen), and pET28. For expression tests, MVP-s constructs were transformed into fresh *Escherichia coli* competent cells and grown overnight in LB medium supplemented with 200 μg/mL AMP and 1% glucose at 37 °C for 12−16 h. Tested *E. coli* strains included XL1-Blue, XL10-Gold, M15, BL21(DE3)pLysS, Rosetta(DE3)pLysS, and Bowie strains 1 and 5 generously provided by R. Nakamoto. The saturated overnight cultures were diluted 100-fold into LB medium with 1% glucose and grown at 37 °C to an OD_{600} of 0.8. The cells were then induced with 1 mM IPTG (Anatrace), and samples of the cultures were taken as they expressed MVP over time. Cell samples were normalized to the amount of cells in the preinduction sample and spun down. Pellets were resuspended in SDS loading dye and broken up by shear force using a syringe fitted with a 30 gauge needle. SDS-solubilized cell samples were loaded for sodium dodecyl sulfate−polyacrylamide gel electrophoresis (SDS−PAGE) and developed for Western blotting. The penta-His antibody (Qiagen) was used as the primary antibody for pET28 and pQE-60, the RGS-His antibody (Qiagen) for pQE-32, and a GST antibody (GE Healthcare) for pGEX-6p-1. In all cases, the secondary antibody was anti-mouse Alexa Fluor 647, followed by detection on an Odyssey Infrared Imaging System (LI-COR). Expression levels were compared roughly by intensities from Western blots. Initial expression conditions were further optimized for *E. coli* strain temperature, IPTG amount, and expression time, following the procedures described above.

The two native cysteine residues at positions 136 and 141 were mutated to serine by site-directed mutagenesis methods using standard procedures to produce cysteine-less MVP-s. This construct was then used as a template to generate single-cysteine mutants for fluorescence and EPR studies.

Detergent Screen. Fresh XL10 competent cells were transformed with MVP-s/pQE-60 and grown in XL10-Gold cells following the methods described for expression tests. The membrane fraction from a large-scale expression was resuspended in buffer A [150 mM KCl and 50 mM Tris (pH 8)] with

dx.doi.org/10.1021/bi4014243 | *Biochemistry* 2014, 53, 1627−1636

protease inhibitor phenylmethanesulfonyl fluoride (PMSF, 1 mM) and homogenized. The membranes were pelleted at 100000*g* for 35 min, and the pellet was resuspended in buffer A and divided into eight aliquots. The eight detergents were individually added at 10 times their critical micellar concentration and incubated at room temperature, rotating, for 2 h. The samples were then spun down at 100000*g* for 35 min, and the supernatant was subjected to SDS−PAGE and Western blot analysis as described for expression tests.

Purification. Fresh BL21(DE3)pLysS competent cells were transformed with MVP-s/pET15b and grown overnight in LB with 1% glucose and 200 μg/mL ampicillin. Overnight cultures were diluted 100-fold in TB medium with 1% glucose and 200 μg/mL ampicillin. Cells were grown for 2.5−3 h to an OD_{600} of 0.5−0.6 and shifted to 30 °C. When the OD_{600} reached 0.8−0.9, the cells were induced with 0.5 mM IPTG. After growing for 5 h at 30 °C, cells were harvested and lysed in buffer A [150 mM KCl and 50 mM Tris (pH 8)] with protease inhibitors phenylmethanesulfonyl fluoride (1 mM), leupeptin (1 μg/mL), pepstatin (0.1 μg/mL), and aprotinin (1 μg/mL). DNase (0.1 mg/mL) and $MgCl_2$ (5 mM) were added to aid homogenization. The mixture was homogenized and spun down at 100000*g* for 35−60 min. MVP was extracted from the membrane pellet with DDM [6−9 mM, *n*-dodecyl β-D-maltopyranoside (Anatrace)] at room temperature for 1−2 h in buffer A with 1 mM PMSF. The extraction mixture was incubated with Talon Co^{2+} affinity resin for 30 min. The resin was collected in a plastic column and washed (buffer A with 15 mM imidazole), and the protein was eluted from the resin (buffer A with 400 mM imidazole and 1 mM DDM). The protein was further purified over a Sephadex-200 HR 10/30 size-exclusion column (GE Healthcare) in an AKTA FPLC system in buffer A with 0.5 mM DDM.

Protein Characterization. The stability of MVP in various detergents was analyzed by exchanging purified MVP with detergents DM, OG, Anzergent 3-14, LDAO, and Foscholine-14. The Superdex 200 HR 10/30 column was individually pre-equilibrated with various detergents, and roughly 100 μg of purified MVP-s was loaded. The elution profile was then evaluated for maintenance of the tetramer peak. Detergents in which MVP-s continued to appear as a monodisperse peak were reinjected, and the elution profile was reevaluated.

The molecular mass and homogeneity of MVP-s−detergent complexes were determined by multiple-angle light scattering (MALS) methods. An AKTA FPLC system equipped with a Superdex 200 HR 10/30 size-exclusion column was coupled to a MALS system with a flow cell. Light scattering was detected with a HELEOS system (Wyatt Technology Corp.) equipped with a 60 mW GaAs laser at 658 nm and 18 detectors at angles from 22.5° to 147.0°. The refractive index was determined from an Opilab rEX unit (Wyatt Technology Corp.). The UV absorbance was measured at 280 nm by the detector from the AKTA system (GE Healthcare) and converted to analog between 0 and 1 V in the HELEOS system. Data were acquired and analyzed using the ASTRA software package (Wyatt Technology Corp.). Both the molecular mass of the protein−detergent complex and the protein content of the complex were analyzed for the peak of interest by the system template Protein Conjugate of ASTRA.

Mutagenesis and Labeling. Cysteine mutants of MVP were grown and purified as described for the wild type (WT) with the addition of 5 mM BME to the lysis and extraction mixtures, and the addition of 0.5 mM TCEP [tris(2-carboxyethyl)phosphine hydrochloride] to the washing buffer and 0.1 mM TCEP to the elution buffer for cobalt column purification. After cobalt affinity purification, they were labeled with either fluorescein 5-maleimide methyl and tetramethylrhodamine 5-maleimide for fluorescence experiments or methanethiosulfonate spin probe [1-oxyl-2,2,5,5-tetramethylpyrrolidin-3-yl (Toronto Research)] for EPR spectroscopy. We labeled the MVP by adding a label to the sample at a 10:1 (label:channel) molar ratio, incubating the reaction mixture on ice for 30 min, adding an additional equal amount to the reaction mixture, and incubating the reaction mixture on ice for at least 30 min again. For fluorescent labels, the sample was incubated instead at room temperature, rotating, for 1 h. The reaction was then quenched with cysteine (10-fold molar excess) and labeled MVP separated from free spin-label or fluorescent label by purification over a PD-10 desalting column (GE Healthcare). Less stable mutants were purified over a Sephadex-200 size-exclusion column in buffer A with 0.5 mM DDM to isolate the tetrameric form.

Fluorescence Spectroscopy. MVP K4C (C136S/C141S) was purified and individually labeled with either fluorescein 5-maleimide ($excitation_{max}$ = 494 nm; $emission_{max}$ = 518 nm) or tetramethylrhodamine 5-maleimide ($excitation_{max}$ = 544 nm; $emission_{max}$ = 572 nm) fluorescent dye. The individually labeled MVP K4C was mixed at a 1:1 donor:acceptor ratio and reconstituted into liposomes of asolectin, *E. coli* extract, or POPC and POPG (3:1). Liposomes were prepared from stock lipids in chloroform following standard protocols: lipids in chloroform were dried on rotovap for 30−60 min, dried under N_2 for 30 min, and diluted to 10 mg/mL with buffer A before being sonicated in a water bath. Concentrated MVP samples were diluted in buffer A with 0.36 mM DDM (2 times the CMC) and added to an equal volume of 10 mg/mL liposomes. The mixture was allowed to incubate at room temperature for 1 h, rotating, before being diluted to 10 mL with buffer A. Detergent was removed by adding Bio-Beads SM-2 Adsorbants (Bio-Rad) and allowing the mixture to incubate overnight. Liposomes were collected by spinning down the mixture at 60000 rpm. The degree of aggregation of MVP was determined by an established fluorescence energy transfer method.[15−18] The fluorescence emission was recorded from 500 to 700 nm upon excitation at 494 nm in a PTI fluorimeter (PTI Technology). The relative FRET intensity in the 570−580 nm range was used as an indicator of the proximity of the donor and acceptor and, by extension, the relative aggregation level of MVP tetramers. Lipid compositions, protein:lipid ratios, and the stability versus time were tested and optimized for minimal FRET values.

Patch-Clamp and Single-Channel Recordings. Electrophysiological measurements of proteoliposomes were made using the patch-clamp method as previously described.[19] MVP-n and MVP-s were reconstituted into asolectin vesicles at channel:lipid molar ratios of 1:100000 to 1:10000 to obtain recordings suitable for single-channel analysis using the procedure described for fluorescence spectroscopy. The proteoliposomes were spun down at 60000 rpm for 1 h and resuspended in 120 μL of 5 mM MOPS (pH 7) and 150 mM KCl. The resuspended proteoliposomes were dried overnight at 4 °C under vacuum and then rehydrated with 5 mM MOPS (pH 7) and 150 mM KCl for 1 h at room temperature. Single-channel recordings were made in inside-out configurations under steady-state conditions. Patch pipettes were pulled from thin-walled borosilicate capillaries, coated with Sylgard (Dow Corning Corp.), and fire-polished to a final resistance of 2−3 MΩ. Currents were recorded under symmetrical conditions of 5 mM MOPS (pH 7.0) and 150 mM KCl buffer. Single-channel currents were recorded using an Axon 200-B patch-clamp

dx.doi.org/10.1021/bi4014243 | *Biochemistry* 2014, 53, 1627−1636

Table 1. Expression of Native and Codon-Optimized MVP Sequences in Various Constructs and Cell Lines[a]

sequence	affinity tag	vector	promoter	*E. coli* strain	relative intensity	yield (mg/L)
MVP-n		pQE-32	T5	XL10-Gold	+	0.125
MVP-s	N-terminal His	pQE-32	T5	XL1-Blue	+++*	
	N-terminal His	pQE-32	T5	XL10-Gold	+++*	
	N-terminal His	pQE-32	T5	M15	+	
	C-terminal His	pQE-60	T5	XL1-Blue	+	
	C-terminal His	pQE-60	T5	XL10-Gold	++++	0.7−1
	C-terminal His	pQE-60	T5	M15	+	
	N-terminal GST	pGEX-6p-1	T5	XL1-Blue	+	
	N-terminal GST	pGEX-6p-1	T5	XL10-Gold	−	
	N-terminal GST	pGEX-6p-1	T5	M15	+	
	N-terminal His	**pET15b**	**T7**	**BL21(DE3)pLysS**	++++	**1.5−2**
	N-terminal His	pET15b	T7	Rosetta(DE3)pLysS	+	
	N-terminal His	pET15b	T7	Exp1-Bowie	+	
	N-terminal His	pET15b	T7	Exp5-Bowie	+	
	C-terminal His	pET28	T7	Exp1-Bowie	−	
	C-terminal His	pET28	T7	Exp5-Bowie	−	

[a]Native and synthetic sequences of MVP were cloned into various expression vectors and assayed for expression in various cell lines by Western blot. Positive (+) and negative (−) signs indicate the relative appearance of MVP bands. Multiple signs indicate relatively higher intensities. Asterisks denote a high level of expression with proteolysis. Some conditions were grown full scale and purified as described in Experimental Procedures; the average yields of these conditions are listed here. Shown in bold is the expression system ultimately chosen for optimization.

amplifier (Axon Instruments, Inc.). The data were digitized at a sampling rate of 40 kHz and low-pass-filtered to 5 kHz through an eight-pole Bessel filter.

EPR Spectroscopy and Analysis. For EPR experiments, labeled MVP was reconstituted at a 1:1500 (protein:lipid) molar ratio in POPC/POPG (3:1) liposomes. Liposomes were prepared from stock lipids in chloroform following standard protocols in 10 mg/mL stock solutions. Samples were reconstituted by adding MVP diluted in buffer A with 0.35 mM DDM (2 times the CMC) to an equal volume of 10 mg/mL POPC/POPG liposomes {3:1 1-palmitoyl-2-oleoyl-*sn*-glycero-3-phosphocholine/1-palmitoyl-2-oleoyl-*sn*-glycero-3-[phospho-*rac*-(1-glycerol)] (Avanti)}. The mixture was allowed to incubate at room temperature for 1 h, rotating, before being diluted to 10 mL with buffer A. Detergent was removed by adding Bio-Beads SM-2 Adsorbants (Bio-Rad) and allowing the mixture to incubate overnight. Liposomes were collected by spinning down the mixture at 60000 rpm. Continuous-wave EPR (CW-EPR) spectroscopic measurements were performed at room temperature on a Bruker EMX X-band spectrometer equipped with a dielectric resonator and a gas-permeable TPX plastic capillary following standard protocols.[15,16,18,20,21] Spectra were recorded at an incident power of 2.0 mW, a modulation frequency of 100 kHz, and a modulation amplitude of 1.0 G.

RESULTS

Expression and Purification of MVP. An optimal expression system for MVP was established after combinatorially screening expression vectors and cell lines. Initially, native MVP (MVP-n) cloned from the genome of *M. jannaschii* was tested for expression in multiple expression vectors with disappointing results (Table 1). However, a synthetic version of MVP (MVP-s), in which 62 of the archaeal codons were altered to bacterial codons (see Experimental Procedures), was successfully expressed in several expression vectors and cell lines (Table 1). Expression levels were qualitatively evaluated by comparing relative intensities of the MVP bands in Western blots of crude cell lysates from small-scale expression trials. The highest yields were obtained using pQE-60/XL10-Gold and pET15b/BL21-(DE3)pLysS expression systems.

Various detergents were assessed for their ability to extract MVP-s from crude membrane fractions by qualitatively comparing intensities of MVP-s bands in clarified extracts (Figure 2A). Western blots of the solubilized crude membrane indicate that all tested detergents extract MVP-s and that MVP-s appears primarily as two major bands around 50 and 20 kDa (Figure 2A). A similar SDS resistance and banding pattern is seen in KcsA, where the higher weight is attributed to the tetrameric form of the channel and the lower weight to monomers.[22] From the relative intensities of these bands, SDS, Anzergent 3-14, and LDAO appear to favor the monomer, while Triton X-100 and DDM stabilize the tetramer. Because of its relatively higher efficiency of extraction and tetramer bias, DDM was chosen for subsequent solubilization during large-scale expression and purification trials.

MVP-s was purified by cobalt affinity and SEC (Figure 2B, pET15b/BL21(DE3)pLysS shown), where fractions containing the tetramer peak exhibited the same major bands via SDS−PAGE as those seen in the Western blots of the detergent screen (Figure 2A). The R_f values for the major two bands are 57.4 ± 0.9 and 21 ± 1 kDa. MVP-s expressed in pET15b/BL21(DE3)pLysS at 30 °C results in 1.5−2 mg/L yields of the channel tetramer, and these channels are stable to reinjection over the course of weeks (Figure 2C). A cysteine-less construct (C136S/C141S) is expressed at WT levels and retains the biochemical properties of the WT construct.

Characterization, Reconstitution, and Function of MVP. Both pQE-60/XL10-Gold and pET15b/BL21(DE3)-pLysS expression systems produced monodisperse peaks eluting around 12 mL (Figure 2C, pET15b/BL21(DE3)pLysS shown). Multiangle light scattering after reinjection via SEC showed that the determined molecular mass of the MVP-s tetramer was 120 ± 10 kDa (Figure 2D), in good agreement with the theoretical molecular mass of the His-tagged MVP-s construct (107.5 kDa). The MVP-s−DDM complex contains approximately 354 DDM molecules per channel at the analyzed concentration of ∼0.8 mg/mL. MVPs appears to be stable only in maltosides, as detergent

dx.doi.org/10.1021/bi4014243 | *Biochemistry* 2014, 53, 1627−1636

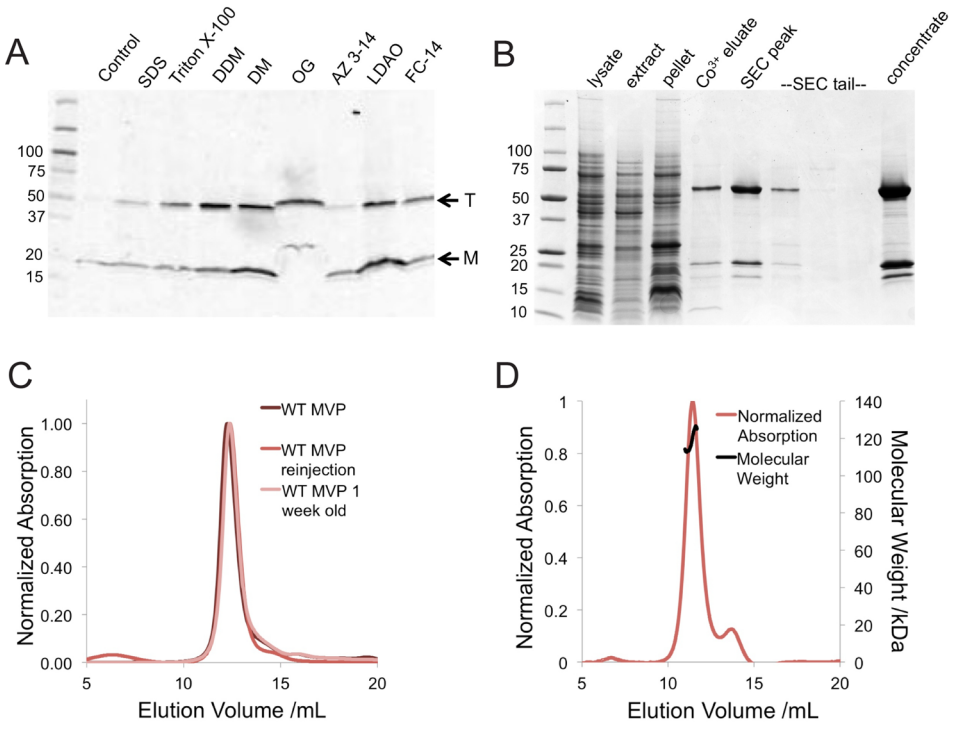

Figure 2. Extraction, purification, and characterization of MVP. (A) Western blot showing a detergent screen of MVP-s in pQE60 expressed in XL10 cells. The control is the MVP membrane fraction with no added detergent. MVP appears as two bands differing in oligomeric state (arrows). Although all tested detergents extracted MVP to a certain extent, DDM was chosen for subsequent purification trials, as it appeared to favor the higher oligomeric state. (B) Coomassie brilliant blue-stained SDS–PAGE gel illustrating the two-step purification process of MVP. The last well was overloaded to highlight impurities. (C) Size-exclusion chromatograph of purified MVP in DDM. The elution volume was ~12 mL on the Superdex 200 HR 10/30 column. (D) MVP's molecular mass determined by multiangle light scattering methods in DDM.

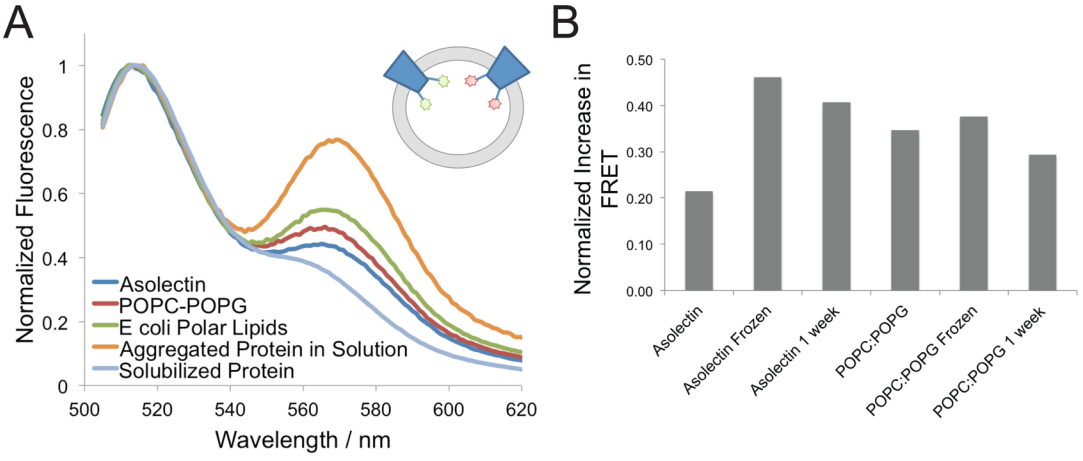

Figure 3. Reconstitution and stability of MVP in liposomes. (A) FRET analysis of N-terminal, fluorescently labeled MVP indicates that MVP can be reconstituted into many lipids and is most stable in asolectin. The inset shows a cartoon of the FRET assay in which tetramers of MVP are separately labeled with either a fluorescent donor or an acceptor and then combined for reconstitution. The strength of the FRET signal indicates the proximity of MVP tetramers and, by extension, the degree of two-dimensional aggregation. (B) Comparison of changes in FRET levels of MVP in different lipids over time. The change in the FRET level was calculated from the difference in the FRET signal intensity under the experimental condition from that of MVP tetramers in detergent (shown in panel A).

exchange tests with FC-12, OG, Anzergent 3-14, or LDAO led to either precipitation before a second reinjection (LDAO) or extreme changes in stability upon reinjection (Anzergent 3-14, FC-12, and OG). Only DM appeared to be able to mimic the stabilizing characteristics of DDM.

Because MVP is an archaeal protein, it is difficult to establish which lipids would create a physiologically relevant membrane environment that best stabilizes the channel and is less likely to promote two-dimensional aggregation. To this end, a simple FRET-based assay[15,17,18,23] was used to estimate relative levels of aggregation of MVP-s tetramers reconstituted in various synthetic, nonarchaeal lipids. In this assay, single-cysteine mutants labeled alternatively with donor or acceptor fluorophores are combined just before reconstitution and assayed for a FRET signal (Figure 3A, inset). For the fluorescein-tetramethylrhodamine (TMR) pair, a strong FRET signal indicates that

dx.doi.org/10.1021/bi4014243 | *Biochemistry* 2014, 53, 1627–1636

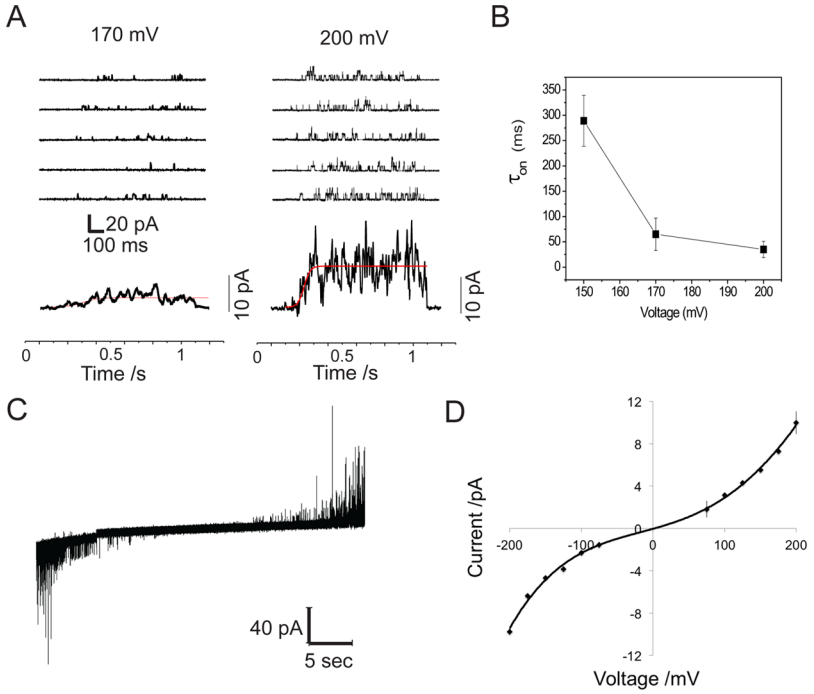

Figure 4. Functional analysis of reconstituted MVP. (A) Traces of MVP-n obtained in symmetric 200 mM KCl (pH 8) at −170 and −200 mV. MVP was reconstituted into asolectin liposomes at a 1:100000 protein: lipid molar ratio. The data were digitized at a sampling rate of 40 kHz and low-pass-filtered to 5 kHz through an eight-pole Bessel filter. Shown below the singles are reconstructions of ensemble measurements from averages of single-channel activity. (B) On kinetics from exponential fits to ensemble currents. (C) Voltage ramp from −200 to 200 mV. Activity at the extreme negative and positive voltages indicates MVP reconstitutes equally in both orientations. (D) *I*−*V* curve constructed from single-channel measurements of reconstituted MVP-s in asolectin liposomes.

the FRET pairs are closer than 50 Å, suggesting that the protein forms small aggregates. The high-magnitude FRET signal from aggregated MVP-s in a detergent-free solution and the low-magnitude FRET signal from solubilized MVP-s exemplify the extremes of this phenomenon (Figure 3A). Cysteine-less MVP-s mutated at the intracellular, N-terminal end of S1 (K4C) was expressed, individually labeled with either fluorescein (donor) or TMR (acceptor), mixed at a 1:1 ratio, and reconstituted in different liposomes. A robust signal from the individually labeled channels in solution suggested that the labeling reaction was efficient. After liposome reconstitution, MVP-s exhibits little or no aggregation in asolectin and POPC/POPG (3:1) liposomes over those made from *E. coli* polar lipids (Figure 3A). Although a lower-magnitude FRET signal was measured for the freshly reconstituted channel in asolectin liposomes than in POPC/POPG liposomes, further experimentation suggested that MVP-s was less likely to aggregate upon freezing or over time in POPC/POPG liposomes, as the FRET signal exhibited little change under these conditions (Figure 3B).

To ascertain whether isolated MVP was functional, we reconstituted the channel into asolectin liposomes at various molar protein:lipid ratios and assayed for single-channel activity using patch-clamp techniques. At low reconstitution ratios (1:100000 to 1:1000000), we obtained singles of MVP at extreme membrane potentials for both native and synthetic constructs (Figure 4A). We were unable to obtain macroscopic currents with either the native or synthetic constructs at high reconstitution ratios, although ensemble activity reconstructions from averaging single-channel conductances reproduced the overall time course of an outward current in which current amplitude and kinetics increase with extreme voltages (Figure 4A,B), confirming that purified MVP exhibits the basic properties expected of a voltage-gated channel. Voltage ramp experiments illustrate that the channels are likely reconstituted equally in both orientations, with similar activity at extremely positive or negative potentials (Figure 4C). The current−voltage (*I*−*V*) plot of MVP-s is hyperlinear (Figure 4D).

Local Structure and Dynamics of the Lower S6 Region. In contrast to standard depolarization-activated channels, MVP should overwhelmingly populate the closed conformation under biochemical conditions at 0 mV because its $V_{1/2}$ is −175 mV (Figure 1C). We set out to spectroscopically evaluate the conformational state of MVP's inner bundle gate by probing the mid to lower S6 region using continuous wave electron paramagnetic resonance (CW-EPR) spectroscopy. The pore domain of potassium channels is well-conserved among family members,[24] and KcsA has been fully characterized by EPR in its open and closed states.[20,21] Therefore, a survey of the local dynamics and degree of intersubunit spin−spin coupling at the S6 helix of MVP-s would provide a direct indication of the overall conformation of MVP's activation gate.

Cysteine mutations were introduced into the cysteine-less construct from position 188 to 209, the last residue of the channel (Figure 5A). This region is located approximately one-third down the length of S6. Cysteine mutants were labeled, reconstituted in POPC/POPG liposomes, and subjected to CW-EPR measurements at 0 mV. EPR spectral line shapes of the S6 residues yielded unique line shapes characteristic of transmembrane regions, confirming the protein is stable and properly folded (Figure 5B). Interestingly, the line shapes of positions 191 and 195 particularly display the particular broadening pattern generated by spin−spin coupling, indicating that the spin-labels on the four subunits are in the proximity of each other (Figure 5B,C, asterisks). This phenomenon is similar to that seen for

dx.doi.org/10.1021/bi4014243 | *Biochemistry* 2014, 53, 1627−1636

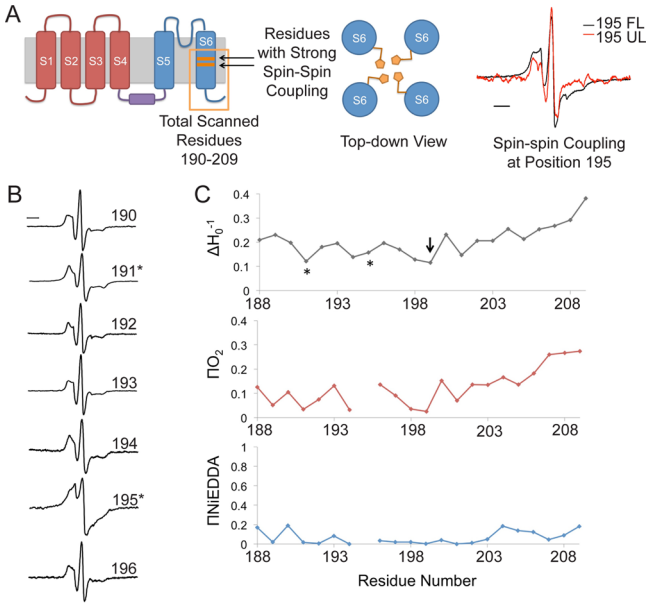

Figure 5. CW-EPR scan of the S6 helix. (A) Schematic showing the membrane topology of MVP, the region scanned for EPR analysis, and a schematic showing how spin-labels on the S6 helix could lie within the proximity of each other in a tetrameric channel. In the far right panel, the amplitude-normalized spectra for fully labeled (FL) and underlabeled (UL; 1:8 label:cysteine) 195C mutants are shown. (B) CW-EPR spectra of residues 190−196 in POPC/POPG liposomes. This region is located about midway through the S6 helix. Asterisks indicate spectra that exhibit strong spin−spin coupling. (C) Plots of the environmental parameters for the S6 region. Asterisks indicate residues whose spectra showed spin−spin coupling; the arrow denotes the point at which the periodicity in the mobility data ends. Environmental parameters were not obtained for residue 195 because the strong spin−spin coupling interfered with this analysis.

EPR measurements of closed channels KcsA[20,21] (see Discussion), MscL,[25,26] and CorA.[27] Such spin−spin coupling patterns have been taken as a clear indication of oligomeric folding in centrosymmetric channels and as evidence of the closed (nonactivated) conformation of the activation gate of ion channels. As illustrated in the far right panel of Figure 5A, when the channel is underlabeled at a ratio of 1:8 (spin-label:tetramer), the line shape loses this characteristic broadening pattern. This is expected if the spectral broadening indeed originates from the interhelix proximity.

In addition, environmental parameters such as mobility (ΔH_0^{-1}) and accessibility to contrast agents Ni-EDDA (ΠNiEDDA) and oxygen (ΠO_2) were obtained from power saturation experiments of the spin-labeled constructs.[28−30] ΔH_0^{-1} is an empirical measure of the local dynamics of the labeled site via the spectral anisotropy affected through tertiary contacts. Positions within loop regions exhibit higher ΔH_0^{-1} values because the spin-label has fewer steric constraints. Positions in transmembrane regions exhibit lower but oscillating ΔH_0^{-1} values because the spin-label may be constrained by contacts with other parts of the protein on different faces of the α-helix. Ni(II)EDDA is a water-soluble chelated paramagnetic ion; therefore, ΠNiEDDA is expected to be high for loop regions that fully exit the membrane interface but extremely low or absent for transmembrane regions. In contrast, given its high solubility in lipids, ΠO_2 is used a reporter for lipidic/membrane-exposed environments.

In the lower region of the S6 helix of MVP-s, ΔH_0^{-1} values oscillate in the expected manner for a transmembrane α helix between positions 188 and 199 and then become increasingly dynamic toward its C-terminus (Figure 5C, arrow). The ΠO_2 trace exhibits similar behavior: it also loses periodicity around position 199 and increases toward the C-terminus. The loss of periodicity likely indicates that around position 199, the S6 helices are no longer packed into a helical bundle with clear protein and lipid interactions. It is at this point that they cross and splay away from each other into the membrane. The S6 helix of MVP is relatively short compared to other potassium channels, and the high ΠO_2 values at the C-terminus may suggest that the intracellular end of the S6 helix does not fully exit the membrane−water interface. In agreement with this, ΠNiEDDA values are consistently low throughout the scanned region (Figure 5C). The low ΠNiEDDA values could be attributed to an underestimation of water accessibility at the membrane−solvent interface, consistent with the fact that the intracellular ends of the S6 segment may be held very close to the membrane−solvent interface. Overall, these data suggest that under these experimental conditions (in POPC/POPG liposomes, in the nominal absence of a membrane potential) the activation gate in MVP's pore domain is in the closed conformation, showing spin-label environmental parameters and spin−spin interaction patterns that are reminiscent of, but distinct from, those of other inner bundle gates in the closed state.

DISCUSSION

Although much progress has been made in determining how Kv channels function at the molecular level, the mechanism underlying electromechanical coupling and the structural basis of reverse polarity coupling in hyperpolarization-activated channels remain poorly understood. It is clear that the underlying nature of inverse gating in both eukaryotic (HCN) and prokaryotic (MVP) systems is not a consequence of altered voltage sensing;[6,8−10] rather, it appears to be directly related to changes in the process of electromechanical coupling between voltage sensors and the gate. So far, structural details for HCN channels are limited to the soluble C-terminal domain, and much of the structural information for the critical transmembrane regions has been obtained from cross-linking studies.[31−35] Here, we report on the biochemical, functional, and EPR conformational characterization of the prokaryotic hyperpolarization-activated potassium channel MVP, focusing on the local structure and dynamics of the lower gate in the closed state at 0 mV.

Closed Conformation of MVP. Because of the high degree of sequence conservation among potassium channel pore domains, our initial approach to characterizing MVP by EPR was to probe the S6 segment, which forms part of the inner helical bundle and defines the activation gate in all Kv channels. This data could then be directly compared to KcsA, a system that has been extensively studied and characterized through a variety of structural and spectroscopic approaches. Overall, we obtained strong signals and characteristically unique line shapes from this region, indicating that the purified and reconstituted MVP preparation represents a properly folded and structurally stable system. Two residues halfway down the S6 segment exhibited distinctive spin−spin coupling, an indication of intersubunit proximity.[20,21,25−27] Residues 191 and 195 are one turn away from each other and appear to line the inner face of the S6 helix, likely participating in the constriction of the lower gate in the closed conformation. Closed KcsA also shows a similar pattern of spin coupling, and these residues were ideal reporters of the pore

dx.doi.org/10.1021/bi4014243 | Biochemistry 2014, 53, 1627−1636

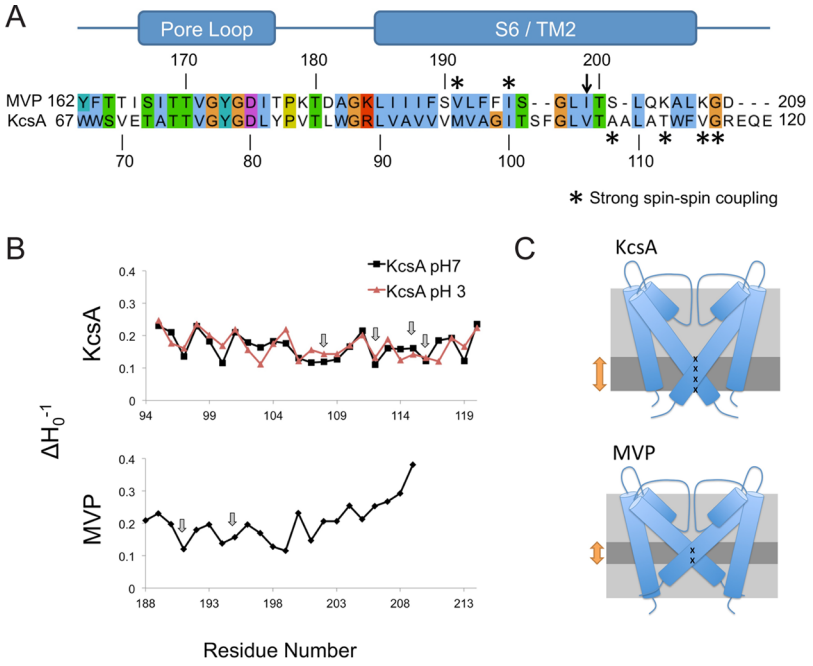

Figure 6. Comparison of KcsA and MVP closed conformations. (A) Alignment of the MVP pore loop and S6 helix (residues 162−209) with the KcsA pore loop and TM2 (residues 67−120). The alignment was made by submitting only the pore TM2 and S6 regions to ClustalW.[46] Asterisks denote residues with strong spin−spin coupling in each channel. The arrow indicates the point at which MVP appears to lose periodicity in its environmental parameters. (B) ΔH_0^{-1} for KcsA in the open (pH 3.5) and closed (pH 7) conformations,[21] and MVP. Arrows denote positions with strong spin−spin coupling. (C) Schematic illustrating the differences observed between the closed conformation of KcsA and MVP. Regions of strong spin−spin coupling for each channel are marked with X's. The channels differ in the region where the strong spin−spin pattern appears, the number of positions with strong spin−spin coupling, and the mobility of the C-terminal ends of the TM2 or S6 segments. This may indicate that MVP's helical bundle crossing occurs closer to the middle of the membrane.

conformation between open (low-pH) and closed (neutral-pH) forms.[20,21]

Sequence alignment and comparison of the EPR data for the two inner bundle helices of MVP and KcsA point to several important observations. First, although it displays considerable sequence similarity, the S6 helix of MVP is somewhat shorter than that of KcsA (Figure 6A). Second, the region that contains strong spin-coupled residues in MVP occurs before the putative glycine hinge in MVP (G197), whereas it occurs after the glycine hinge (G104) in KcsA. This suggests that while the constricted portion of KcsA occurs closer to where TM2 (S6) exits the membrane, in MVP it may occur closer to the middle of the membrane (Figure 6C). A comparison of the mobility profiles along this region in the two channels (Figure 6B) also indicates that the C-terminal end of the pore domain adopts different closed conformations in these channels. KcsA's lower gate probably exhibits low mobility as its exits the membrane because of the extensive, soluble C-terminal domain that constrains the movement of the C-terminal ends of the TM2 region.[19,36,37] In contrast, MVP's lower gate is unconstrained by any C-terminal domain, and the high oxygen and low NiEDDA accessibilities of this region in MVP suggest that the C-terminal ends of the MVP's S6 helix may remain splayed into the bilayer.

Understanding Electromechanical Coupling in Hyperpolarization-Activated Channels. In canonical Kv channels, the transition to the resting potential results in a downward motion of the S4 helix (toward the intracellular side). This downward motion is transmitted to the S4−S5 linker, which is described by current models as exerting a "pushing" force on the lower region of the S6 helix[24,38] leading to pore closure. However, in the hyperpolarization-activated channel (i.e., MVP), the same downward S4 motion leads to channel opening. This hypothesis naturally begs the question of whether in channels with reverse polarity coupling, the function of the S4−S5 linker is to pull the lower gate closed when S4 moves upward (extracellular) or to push it open when S4 moves downward (intracellular). Alignments of various voltage-gated ion channel families have demonstrated divergence among Kv, CNG, and HCN S4−S5 linker regions, suggesting that these channels might couple their VSDs and pore domains in a manner different from that of canonical Kv channels.[39] Alanine-scanning mutagenesis of the S4−S5 linker in HCN2 demonstrated that mutations at residues Y331 and R339 disrupted channel closing.[13] Furthermore, the fact that the S4−S5 linker can be cross-linked to the lower region of the S6 helix[31,33] corroborates the idea that these channels also use the S4−S5 linker to couple the VSD to the pore domain. However, difficulties in mapping these interactions onto existing Kv models suggest that HCN channels most likely gate through a unique coupling mechanism.[31]

By directly probing the local dynamics and residue environmental parameters, we were able to evaluate local structural differences in MVP in reference to KcsA, a model system of known structure and conformation. These differences suggest a distinct closed pore conformation that may have altered interactions with the S4−S5 linker during gating, underlying MVP's reverse polarity coupling. Interestingly, the position at which the S6 segments in MVP appear to cross and leave the helical bundle (residue 199) occurs after the primary glycine hinge in KcsA (G104) (a region that aligns to the PXP sequence in Kv channels[40]). The PXP region has been shown to contact the S4−S5 linker in the crystal structure of the Kv1.2 chimera,[41] and mutating this region in *Shaker* decouples the VSD and pore

dx.doi.org/10.1021/bi4014243 | *Biochemistry* 2014, 53, 1627−1636

domain.[42] It is possible that in MVP the S4−S5 linker still makes contact with the pore domain to couple it to the VSD but that these interactions have been altered to accommodate a modified activation gate. The constricted region in MVP's pore domain is located well before the region in *Shaker* shown to contain the gating residues that are expected to seal the pore in the closed state.[43,44] For MVP, the narrowest constriction in the lower gate occurs in the middle of the S6 helix, instead of at the intracellular side of the membrane (as in KcsA). Furthermore, our accessibility data indicate that the ends of the S6 helices appear to splay into the lower portion of the bilayer. Therefore, the S4−S5 linker may be interacting with the pore domain through a novel mechanism to open the channel when the VSD is in the down state under hyperpolarizing conditions.

Because HCNs have highly structured C-terminal domains that could constrain the conformational freedom of the lower S6 region, they could potentially utilize a different mechanism for regulating the activation gate. However, determining how the VSD is coupled to the pore domain in MVP should nevertheless lay the groundwork for understanding the mechanics of electromechanical coupling in hyperpolarization-activated channels and inform future studies of HCN channels. Our proposed model for the structure of MVP's activation gate is not unprecedented: the recent structure of TRPV1 exhibits an activation gate whose helical bundle also crosses closer to the middle of the membrane.[45] TRP channels are only distantly related to the Kv channels yet display remarkable structural similarity. It is likely that small modifications to the conserved 6TM voltage-gated ion channel architecture underlie large changes in channel behavior and function.

AUTHOR INFORMATION

Corresponding Author

*E-mail: eperozo@uchicago.edu. Phone: (773) 834-4747.

Present Address

[†]L.G.C.: Department of Cell Physiology and Molecular Biophysics, Texas Tech University Health Sciences Center, Lubbock, TX 79430.

Funding

This work was supported in part by National Institutes of Health Grant R01-GM57846 (to E.P.).

Notes

The authors declare the following competing financial interest(s): I receive funding for a collaborative project with Bristol-Myers Squibb. That project is unrelated to the research in this work.

ACKNOWLEDGMENTS

We thank Steve Goldstein for kindly providing the synthetic MVP gene and Francisco Bezanilla for kindly allowing access to the PTI fluorimeter. Many thanks to Ernesto Vargas for writing software that greatly facilitated EPR data analysis. We thank the members of the Perozo lab for helpful discussions and invaluable experimental advice. In particular, Olivier Dalmas and Qufei Li were instrumental in offering helpful advice with EPR data acquisition and troubleshooting.

ABBREVIATIONS

CMC, critical micellar concentration; CNBD, cyclic nucleotide-binding domain; CNG, cyclic nucleotide-gated channel; CW-EPR, continuous wave electron paramagnetic resonance; DDM, dodecyl D-maltoside; DM, decyl D-maltoside; FC-12, Fos-choline-12; FPLC, fast protein liquid chromatography; GST, glutathione *S*-transferase; HCN, hyperpolarization-activated cyclic nucleotide-gated channel; IPTG, isopropyl β-D-thiogalactopyranoside; KcsA, potassium crystallographically sited activation channel; Kv, voltage-gated potassium channel; LDAO, lauryldimethylamine oxide; MVP, *M. jannaschii* voltage-gated protein; NiEDDA, nickel(II)ethylenediamine di(*o*-hydroxyphenylacetic acid); OG, octyl D-glycoside; PCR, polymerase chain reaction; PD, pore domain; POPC/POPG, 3:1 mixture of POPC and POPG; POPC, 1-palmitoyl-2-oleoyl-*sn*-glycero-3-phosphocholine; POPG, 1-palmitoyl-2-oleoyl-*sn*-glycero-3-[phospho-*rac*-(1-glycerol)]; SDS−PAGE, sodium dodecyl sulfate−polyacrylamide gel electrophoresis; SDS, sodium dodecyl sulfate; SEC, size-exclusion chromatography; TCEP, tris(2-carboxyethyl)-phosphine hydrochloride; VSD, voltage-sensing domain; ΔH_0^{-1}, mobility as the inverse width of the central resonance line width of CW-EPR spectra; ΠNiEDDA, Ni-EDDA accessibility; ΠO_2, oxygen accessibility.

REFERENCES

(1) Swartz, K. (2004) Towards a structural view of gating in potassium channels. *Nat. Rev. Neurosci. 5*, 905−916.

(2) Bezanilla, F. (2008) How membrane proteins sense voltage. *Nat. Rev. Mol. Cell Biol. 9*, 323−332.

(3) Catterall, W. (2010) Ion channel voltage sensors: Structure, function, and pathophysiology. *Neuron 67*, 915−928.

(4) Blunck, R., and Batulan, Z. (2012) Mechanism of electromechanical coupling in voltage-gated potassium channels. *Front. Pharmacol. 3*, 166.

(5) Vardanyan, V., and Pongs, O. (2012) Coupling of voltage-sensors to the channel pore: A comparative view. *Front. Pharmacol. 3*, 145.

(6) Sesti, F., Rajan, S., Gonzalez-Colaso, R., Nikolaeva, N., and Goldstein, S. (2003) Hyperpolarization moves S4 sensors inward to open MVP, a methanococcal voltage-gated potassium channel. *Nat. Neurosci. 6*, 353−361.

(7) Bult, C. J., et al. (1996) Complete genome sequence of the methanogenic archaeon, *Methanococcus jannaschii*. *Science 273*, 1058−1073.

(8) Männikkö, R., Elinder, F., and Larsson, H. (2002) Voltage-sensing mechanism is conserved among ion channels gated by opposite voltages. *Nature 419*, 837−841.

(9) Latorre, R., Olcese, R., Basso, C., Gonzalez, C., Munoz, F., Cosmelli, D., and Alvarez, O. (2003) Molecular coupling between voltage sensor and pore opening in the *Arabidopsis* inward rectifier K^+ channel KAT1. *J. Gen. Physiol. 122*, 459−469.

(10) Vemana, S., Pandey, S., and Larsson, H. (2004) S4 movement in a mammalian HCN channel. *J. Gen. Physiol. 123*, 21−32.

(11) Zagotta, W., Olivier, N., Black, K., Young, E., Olson, R., and Gouaux, E. (2003) Structural basis for modulation and agonist specificity of HCN pacemaker channels. *Nature 425*, 200−205.

(12) Craven, K., and Zagotta, W. (2006) CNG and HCN channels: Two peas, one pod. *Annu. Rev. Physiol. 68*, 375−401.

(13) Chen, J., Mitcheson, J., Tristani-Firouzi, M., Lin, M., and Sanguinetti, M. (2001) The S4-S5 linker couples voltage sensing and activation of pacemaker channels. *Proc. Natl. Acad. Sci. U.S.A. 98*, 11277−11282.

(14) Decher, N., Chen, J., and Sanguinetti, M. (2004) Voltage-dependent gating of hyperpolarization-activated, cyclic nucleotide-gated pacemaker channels: Molecular coupling between the S4-S5 and C-linkers. *J. Biol. Chem. 279*, 13859−13865.

(15) Li, Q., Jogini, V., Wanderling, S., Cortes, D., and Perozo, E. (2012) Expression, purification, and reconstitution of the voltage-sensing domain from Ci-VSP. *Biochemistry 51*, 8132−8142.

(16) Chakrapani, S., Cuello, L., Cortes, D., and Perozo, E. (2008) Structural dynamics of an isolated voltage-sensor domain in a lipid bilayer. *Structure (Oxford, U.K.) 16*, 398−409.

(17) Vásquez, V., Cortes, D., Furukawa, H., and Perozo, E. (2007) An optimized purification and reconstitution method for the MscS channel: Strategies for spectroscopical analysis. *Biochemistry 46*, 6766−6773.
(18) Cuello, L., Cortes, D., and Perozo, E. (2004) Molecular architecture of the KvAP voltage-dependent K^+ channel in a lipid bilayer. *Science 306*, 491−495.
(19) Cortes, D., Cuello, L., and Perozo, E. (2001) Molecular architecture of full-length KcsA: Role of cytoplasmic domains in ion permeation and activation gating. *J. Gen. Physiol. 117*, 165−180.
(20) Perozo, E., Cortes, D., and Cuello, L. (1998) Three-dimensional architecture and gating mechanism of a K^+ channel studied by EPR spectroscopy. *Nat. Struct. Biol. 5*, 459−469.
(21) Perozo, E. (1999) Structural Rearrangements Underlying K^+-Channel Activation Gating. *Science 285*, 73−78.
(22) Cortes, D., and Perozo, E. (1997) Structural dynamics of the *Streptomyces lividans* K^+ channel (SKC1): Oligomeric stoichiometry and stability. *Biochemistry 36*, 10343−10352.
(23) Chakrapani, S., Cordero-Morales, J., and Perozo, E. (2007) A quantitative description of KcsA gating I: Macroscopic currents. *J. Gen. Physiol. 130*, 465−478.
(24) Lu, Z., Klem, A., and Ramu, Y. (2001) Ion conduction pore is conserved among potassium channels. *Nature 413*, 809−813.
(25) Perozo, E., Kloda, A., Cortes, D., and Martinac, B. (2001) Site-directed spin-labeling analysis of reconstituted Mscl in the closed state. *J. Gen. Physiol. 118*, 193−206.
(26) Perozo, E., Cortes, D., Sompornpisut, P., Kloda, A., and Martinac, B. (2002) Open channel structure of MscL and the gating mechanism of mechanosensitive channels. *Nature 418*, 942−948.
(27) Dalmas, O., and Perozo, E. (2011) Structural Rearrangements Underlying Mg^{2+} Dependent Gating in Cora. *Biophys. J. 100*, 272a.
(28) Mchaourab, H., Lietzow, M., Hideg, K., and Hubbell, W. (1996) Motion of spin-labeled side chains in T4 lysozyme. Correlation with protein structure and dynamics. *Biochemistry 35*, 7692−7704.
(29) Altenbach, C., Froncisz, W., Hyde, J., and Hubbell, W. (1989) Conformation of spin-labeled melittin at membrane surfaces investigated by pulse saturation recovery and continuous wave power saturation electron paramagnetic resonance. *Biophys. J. 56*, 1183−1191.
(30) Farahbakhsh, Z., Altenbach, C., and Hubbell, W. (1992) Spin labeled cysteines as sensors for protein-lipid interaction and conformation in rhodopsin. *Photochem. Photobiol. 56*, 1019−1033.
(31) Kwan, D., Prole, D., and Yellen, G. (2012) Structural changes during HCN channel gating defined by high affinity metal bridges. *J. Gen. Physiol. 140*, 279−291.
(32) Ryu, S., and Yellen, G. (2012) Charge movement in gating-locked HCN channels reveals weak coupling of voltage sensors and gate. *J. Gen. Physiol. 140*, 469−479.
(33) Prole, D., and Yellen, G. (2006) Reversal of HCN channel voltage dependence via bridging of the S4-S5 linker and Post-S6. *J. Gen. Physiol. 128*, 273−282.
(34) Rothberg, B., Shin, K., Phale, P., and Yellen, G. (2002) Voltage-controlled gating at the intracellular entrance to a hyperpolarization-activated cation channel. *J. Gen. Physiol. 119*, 83−91.
(35) Rothberg, B., Shin, K., and Yellen, G. (2003) Movements near the gate of a hyperpolarization-activated cation channel. *J. Gen. Physiol. 122*, 501−510.
(36) Uysal, S., Vásquez, V., Tereshko, V., Esaki, K., Fellouse, F., Sidhu, S., Koide, S., Perozo, E., and Kossiakoff, A. (2009) Crystal structure of full-length KcsA in its closed conformation. *Proc. Natl. Acad. Sci. U.S.A. 106*, 6644−6649.
(37) Uysal, S., Cuello, L., Cortes, D., Koide, S., Kossiakoff, A., and Perozo, E. (2011) Mechanism of activation gating in the full-length KcsA K^+ channel. *Proc. Natl. Acad. Sci. U.S.A. 108*, 11896−11899.
(38) Lu, Z., Klem, A., and Ramu, Y. (2002) Coupling between voltage sensors and activation gate in voltage-gated K^+ channels. *J. Gen. Physiol. 120*, 663−676.
(39) Anselmi, C., Carloni, P., and Torre, V. (2007) Origin of functional diversity among tetrameric voltage-gated channels. *Proteins 66*, 136−146.
(40) Del Camino, D., Holmgren, M., Liu, Y., and Yellen, G. (2000) Blocker protection in the pore of a voltage-gated K^+ channel and its structural implications. *Nature 403*, 321−325.
(41) Long, S., Campbell, E., and Mackinnon, R. (2005) Voltage sensor of Kv1.2: Structural basis of electromechanical coupling. *Science 309*, 903−908.
(42) Haddad, G., and Blunck, R. (2011) Mode shift of the voltage sensors in Shaker K^+ channels is caused by energetic coupling to the pore domain. *J. Gen. Physiol. 137*, 455−472.
(43) Ding, S., and Horn, R. (2002) Tail end of the s6 segment: Role in permeation in shaker potassium channels. *J. Gen. Physiol. 120*, 87−97.
(44) Hackos, D., Chang, T.-H., and Swartz, K. (2002) Scanning the intracellular S6 activation gate in the Shaker K^+ channel. *J. Gen. Physiol. 119*, 521−532.
(45) Cao, E., Liao, M., Cheng, Y., and Julius, D. (2013) TRPV1 structures in distinct conformations reveal activation mechanisms. *Nature 504*, 113−118.
(46) Larkin, M. A., Blacksheilds, G., Brown, N. P., Chenna, R., McGettigan, P. A., McWilliam, H., Valentin, F., Wallace, I. M., Wilm, A., Lopez, R., Thompson, J. D., Gibson, T. J., and Higgens, D. G. (2007) ClustalW and ClustalX version 2. *Bioinformatics 23*, 2947−2948.